Colloids and Surfaces A: Physicochemical and Engineering Aspects 655 (2022) 130167

Contents lists available at ScienceDirect

Colloids and Surfaces A: Physicochemical and Engineering Aspects

journal homepage: www.elsevier.com/locate/colsurfa

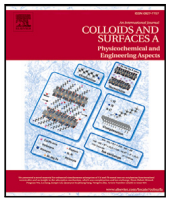

Estimates of noble metal particle growth in a molten salt reactor

E.M.A. Frederix

Nuclear Research and Consultancy Group (NRG), Westerduinweg 3, 1755 LE, Petten, The Netherlands

GRAPHICAL ABSTRACT

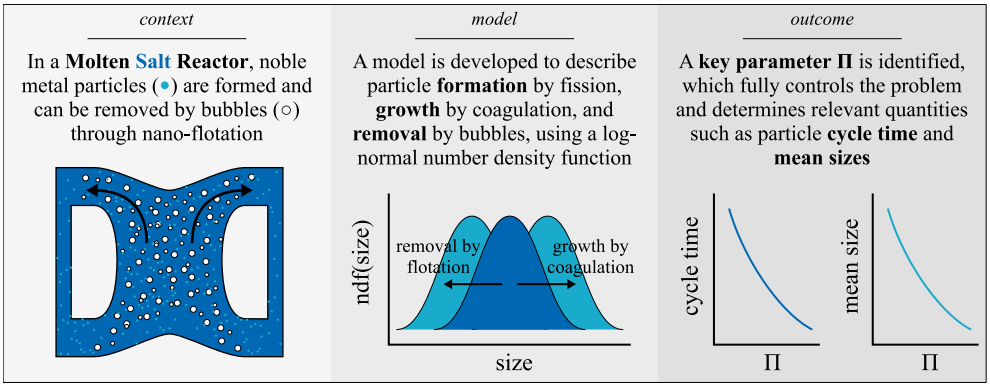

ARTICLE INFO

Keywords:
Nano-flotation
Molten salt reactor
Interfacial processes
Modeling

ABSTRACT

Within the H2020-Euratom project SAMOSAFER, research is currently ongoing into the Molten Salt Fast Reactor (MSFR) concept in which nuclear fuel is dissolved in a liquid salt. A major challenge in the MSFR is the online and offline treatment of salt in order to remove a plethora of fission products. Noble metals are a type of such fission products, the atoms of which are thought to coagulate into particles as a result of diffusion. Due to their low solubility, noble metal particles will deposit onto interfaces such as solid walls but also on bubbles, as was observed in the Molten Salt Reactor Experiment (MSRE) at Oak Ridge national laboratory. The relatively large interfacial area generated by bubbles makes online or offline bubbling, therefore, an interesting option to extract noble metals from the MSFR and to limit wall deposition. However, to understand the performance of the bubbling process, particle sizes must be known. Particle size distributions arise from a complex interplay of atomic formation by fission and decay, growth by coagulation and removal by interfacial deposition. In this paper, theory is developed to understand these mechanisms on a semi-analytical level, in order to provide estimates of noble metal particle growth in the MSFR. The governing partial differential equation is reduced to a set of ordinary differential equations using the method of moments, revealing the dynamics of the underlying physics. We show that large noble metal particles, up to the micrometer scale, can arise in the reactor, but only at very long operational times. Moreover, we show that the previously assumed 'cycle time' of noble metal particle removal of 30 s is only feasible at very high bubbling void fractions. The theory developed in this work contributes significantly to a qualitative understanding of the behavior of noble metals in an MSR. The theory can potentially help to explain certain phenomena observed in the MSRE and can assist in the future design of safe and reliable MSRs.

E-mail address: frederix@nrg.eu.

https://doi.org/10.1016/j.colsurfa.2022.130167
Received 1 August 2022; Received in revised form 31 August 2022; Accepted 10 September 2022
Available online 21 September 2022

1. Introduction

Molten Salt Reactors (MSRs) are a type of nuclear reactor in which a molten salt is used as the primary coolant held at a high temperature, either to remove heat from conventional solid fuel assemblies or from fuel that is dissolved in the salt itself. An important benefit of using molten salt as a coolant is its high heat capacity and high boiling point, allowing for efficient operation at near-atmospheric pressure. Advantages of fluid-fueled reactors are a high thermal expansion coefficient providing inherent safety, the possibility of continuous and batch fuel reprocessing and better resource utilization, as transuranic elements can be cycled through the core to eventually undergo fission [1]. In this work, as part of the H2020-Euratom SAMOSAFER project, we focus on the fluid-fueled MSR concept, and in particular on the MSFR concept [2].

When fuel is dissolved in the salt, its fission products will form and decay inside the salt too. In the context of MSRs, fission products can be categorized into three groups: salt seekers, noble gases and noble metals [3]. Salt seekers tend to dissolve in the salt as they form stable bonds with fluorine. Noble gases (typically Xe and Kr) and noble metals do not, and have extremely low solubility in the salt. As such, they migrate to salt–gas and salt–solid interfaces, where they deposit. In the case of salt–solid interfaces, noble metals are very likely to adhere to the solid surface permanently, particularly on metal surfaces. This process is called *plating*, and can lead to dangerous hot spots in power reactor systems as a result of decay heat, even more so in loss-of-coolant accident scenarios. The behavior of noble gases and noble metals, being a subject of major importance to the design of MSRs, was already extensively studied half a century ago, in the Molten Salt Reactor Experiment at Oak Ridge National Lab., e.g., see [3,4]. It was observed that when helium bubble entrainment into the salt increased (which, in fact, was unintended) from 0.04% to 0.5% void fraction, noble metal deposition shifted significantly from the vessel and heat exchanger walls towards the off-gas system [5]. This resulted in 86% of the total noble metal mass to be deposited in the pump bowl, overflow tank or off-gas system, suggesting that salt bubbling can be leveraged as a tool to control and reduce noble metal plating. To explain the results observed in the MSRE, we speculate that the tendency of noble metals to adhere to bubbles is likely to be amplified because of three reasons. First, bubbles have a relative velocity with respect to the salt as a result of buoyancy or other forms of drift. This, in turn, enhances mass transfer as expressed by an increase in the Sherwood number as a function of bubble Reynolds number and particle Schmidt number. Thus, per unit of interfacial area, bubbles could be likely to absorb noble metals more efficiently than solid walls. Second, most noble metals will form in the core of the reactor where the fission rate is highest, relatively far away from solid walls but close to bubbles that can freely drift and rise into the core. Therefore, noble metals are more likely to encounter a bubble before they reach a solid wall. Third, the interfacial area concentration of bubbles can be made larger than that of walls. For example, in the MSRE the total area of walls (excluding the graphite moderator, which is not used in the MSFR) was about 80 m^2 [6] enclosing a total salt volume of about 2 m^3 [3], giving a wall area concentration of 40 m^{-1}. The wall area concentration will reduce further for larger salt volumes such as that of the MSFR (18 m^3). On the other hand, the interfacial area concentration of 1 mm bubbles at a void fraction of 1% is 60 m^{-1}. This is independent of the salt volume and will dominate wall area concentration at larger salt volumes, thus leading to a preference of particles to attach to bubbles instead of walls. These considerations, then, are a strong motivation to explore the use of an online bubbling system in MSRs, as is indeed envisaged in the MSFR [7].

Noble metals are thought to originate as, or very rapidly become, individual metal atoms and diffuse in the salt as such [5]. Because they have low solubility, aggregation of atoms into colloidal particles, and subsequent aggregation of such particles into larger ones, is likely. Just like atoms, small metal particles undergo diffusion too, however, this colloidal diffusion is usually referred to as *Brownian diffusion*. The Stokes–Einstein equation modeling Brownian diffusivity is proportional to $1/d$ with d the particle diameter, showing that diffusive mobility decreases with size. The flux of noble metal particles thus becomes a function of size, making the net rate of particle absorption by bubbles a non-trivial integral over the complete size spectrum of coagulated particles. The idea of diffusion-driven noble metal particle absorption by bubbles, here referred to as *diffusional flotation*, carries an obvious similarity with classical heat and mass transfer theory. While MSRE research into noble metal behavior was significantly hampered by the complexities associated with the operation of an integral reactor system, the hypothesis that noble metals migrate according to the simplest form of mass transfer theory has always prevailed and is supported by experimental evidence [3,6,8].

In addition to diffusional transport, from classical flotation theory [9] it is known that for particles with sizes beyond 100 nm, hydrodynamic effects contribute to particle–bubble absorption too. Large particles can sediment due to gravity, or drift due to inertia. Consequently, that leads to an enhancement in the likelihood of particle–bubble collision. The magnitude of *hydrodynamic flotation* typically carries a proportionality with the Stokes number which, in turn, is proportional to d^2. Thus, the total flotation efficiency curve, from the nanometer scale up to the millimeter scale, is expected to be V-shaped where the left 'arm' is diffusion-driven and the right 'arm' is hydrodynamics-driven. The presence of a minimum in the flotation efficiency curve has been experimentally observed for silica particles in water, see [10].

So, the flotation efficiency curve is expected to be a strong function of particle size, where particle sizes can span several orders of magnitude. The prevailing underlying mechanism of flotation, being diffusion or hydrodynamics, is not know a priori. Therefore, estimates of the noble metal particle size distribution, subject to the operating conditions inside the reactor, should be developed. In this work, we do this by considering the classical particle coagulation equation amended by an additional source and sink term to account for particle formation as a result of fission or precursor decay, and removal by bubbles, respectively. We show that the process of particle formation and particle removal is closely linked with two time scales: one of growth and one of removal. An evaluation of the two readily provides estimates of the equilibrium particle size spectrum at which the rate of particle production is balanced by the rate of removal. The equilibrium removal rate gives rise to a cycle time, i.e., the mean life time of noble metal atoms in the reactor between production by fission or decay and removal by bubbles. The developed theory relies on the assumption that the particle size distribution is log-normal. This reduces the complexity of the model significantly, but preserves the fundamental dynamics inherent to the problem at hand, including knowledge on the moments of the particle size distribution. Finally, we apply the developed theory to estimates of operational parameters of the MSFR, giving insight in the process of noble metal particle formation in operational conditions.

The structure of this paper is as follows. In Section 2, we consider the situation in which particles are not removed from the system and are free to agglomerate. Next, in Section 3, we consider the opposite: particle removal without production. The resulting models are then combined in Section 4, allowing to make a first realistic estimate of particle sizes in the MSFR. Finally, in Section 5 we formulate the conclusions of this work.

2. Noble metal particle size spectra without sinks

We study the formation and coagulation of noble metal particles in the context of an imaginary infinitely large and homogeneous MSR, first without any bubbles or other surfaces on which particles can deposit. Without any depositories, the growth of particles due to coagulation will be indefinite, assuming that they will not decay further. Nevertheless, the approach developed in this section will serve as a basis for further analysis of the complete problem that will be addressed later on.

2.1. Modeling the noble metal particle spectrum

Noble metal atoms are born in a nuclear reactor as the result of fission or from the decay of precursors. Their solubility in the salt is very low. For example, measurements in the MSRE showed that only 0.21% of the total ^{99}Mo mass produced in the reactor was found in the salt. Everything else had deposited on the graphite moderator, metal walls or in the purge gas system [5]. Drawing an analogy with Classical Nucleation Theory (CNT), the low solubility of noble metal atoms in salt can be considered as an over-saturation leading to the formation of critical clusters whose probability of further growth equals that of disappearance. However, whereas in CNT such clusters usually consist of a relatively large number of atoms, here we assume that the 'critical clusters of noble metal atoms' consist of just one atom as a consequence of strong insolubility. This is analogous to condensable materials with very low vapor pressures, in which essentially all collisions are effective so that the critical cluster size is a single molecule [11]. This assumption, which is supported by the experimental evidence from the MSRE, allows us to avoid the modeling of formation of the metallic particle analogy of a critical cluster. Instead, we may directly inject single atoms in the population of noble metal particles, as single-atom particles.

We introduce the population $n(v,t)$ with particle volume v and time t, defined in such a way that $n(v,t)\mathrm{d}v$ provides the total number concentration of particles having a particle volume in the interval $[v, v+\mathrm{d}v]$. The population is not yet affected by any sinks, but undergoes 'nucleation' of new particles and coagulation due to Brownian diffusion. Its evolution in time is subject to the population balance equation given by

$$\begin{aligned}\frac{\partial n(v,t)}{\partial t} &= \frac{1}{2}\int_0^v \beta(v-u,u)n(v-u,t)n(u,t)\mathrm{d}u \\ &- n(v,t)\int_0^\infty \beta(v,u)n(u,t)\mathrm{d}u \\ &+ \delta(v-w)F,\end{aligned} \tag{1}$$

with $\beta(u,v)$ the collection kernel (e.g., see [12–14]) which will be clarified momentarily, w the volume of a single noble metal atom and F the rate at which noble metal atoms are born per unit of volume. The rate F is assumed to be a constant, implying that the reactor operates at steady state in terms of neutronics. The first term in the right-hand side is the rate at which particles of size v are formed as a result of binary coagulation of particles of size $v-u$ and u. The second term is the rate at which particles of size v are lost due to coagulation into bigger ones. The third term is the formation rate, modeled by a Dirac delta function shifted to the atomic volume w.

In principle, we can introduce a population balance Eq. (1) for each noble metal isotope and track the evolution of each size distribution separately. However, this is problematic for two reasons. First, some noble metal isotopes are short-lived, meaning that they decay into other elements. To account for this, a decay sink term should be included into (1), which is not straight-forward due to the large number of decay chains. Second, noble metal particles are likely to consist of a spectrum of elements, essentially demanding a high-dimensional multi-species population balance model. To avoid these difficulties, we consider noble metal formation as a single-species problem with material properties appropriately averaged over all individual isotopes. Moreover, it is assumed that when a noble metal atom decays, it decays into another lower noble metal atom, therewith not significantly changing its properties. This, then, allows us to retain (1), in which the population $n(v,t)$ now pertains to the population of all multi-species noble metal particles subject to an assumption of 'internal mixing', i.e., their composition is independent of v. Of course, the real decay of noble metals will include a variety of decay chains, some of which will result in salt seekers, therewith removing mass from the population. This will be particularly relevant when the time scale of particle growth is much larger than that of decay into salt seeking elements. Thus, the neglect of this removal term implies that the developed model will produce an upper bound in terms of particle sizes. Similar to the removal term of particles by bubbles as will be introduced in Section 3, a term for removal by decay can also be introduced. However, this is left for future research.

The collection kernel $\beta(u,v)$ provides the rate at which particles of volume u collide and coagulate with particles of volume v. In the problem at hand, collisions are driven by the Brownian motion of particles. The Knudsen number, expressing the ratio of the mean free path in the salt over the particle size, is expected to be much smaller than unity, which is generally true for particles suspended in a liquid [13]. Following [13], the collection kernel then takes the form

$$\beta(u,v) = K(\sqrt[3]{u}+\sqrt[3]{v})(1/\sqrt[3]{u}+1/\sqrt[3]{v}) = K[2+\sqrt[3]{u/v}+\sqrt[3]{v/u}] \tag{2}$$

where K is the coagulation constant given by

$$K = \frac{2kT}{3\mu} \tag{3}$$

with Boltzmann constant k, temperature T and salt dynamic viscosity μ. The coagulation constant is related to the Stokes–Einstein diffusivity D as $K = 2\pi d D$ and has units m^3/s.

Solving the partial differential Eq. (1) subject to (2) explicitly for $n(v,t)$ is not straightforward and can only be done numerically. A full discretization in volume space, covering many decades, must be adopted (e.g., see [15–17]), however, this would not yield any fundamental insight into the dynamics of the model. Here, instead of pursuing such an approach, we reduce the problem by considering moments of the size distribution only. The γth volume moment is defined as

$$M_\gamma(t) = \int_0^\infty v^\gamma n(v,t)\mathrm{d}v. \tag{4}$$

From the moments, we can extract useful information pertaining to the evolution of the size distribution, such as mean size and variance. Multiplying (1) by v^γ, integrating over $[0,\infty)$ in v and introducing (2) and (4), gives

$$\begin{aligned}\frac{\mathrm{d}M_\gamma(t)}{\mathrm{d}t} &= \frac{K}{2}\int_0^\infty\int_0^\infty [(u+v)^\gamma - u^\gamma - v^\gamma][2+\sqrt[3]{u/v} \\ &+ \sqrt[3]{v/u}]n(u,t)n(v,t)\mathrm{d}u\mathrm{d}v + w^\gamma F,\end{aligned} \tag{5}$$

where the first two terms in the right-hand side of (1) have been combined, see [12]. For the number concentration ($\gamma = 0$), the volume concentration ($\gamma = 1$) and the squared volume concentration ($\gamma = 2$) the general moment balance equations become

$$\frac{\mathrm{d}M_0}{\mathrm{d}t} = -K[M_0^2 + M_{1/3}M_{-1/3}] + F, \tag{6a}$$

$$\frac{\mathrm{d}M_1}{\mathrm{d}t} = wF \tag{6b}$$

and

$$\frac{\mathrm{d}M_2}{\mathrm{d}t} = 2K[M_1^2 + M_{4/3}M_{2/3}] + w^2F, \tag{6c}$$

respectively, where we have rewritten the integrals over the polynomial-weighted size distribution in terms of the moments using (4). We recall that M_γ is only a function of time for any γ. With M_1 being the volume fraction of particles, we observe from (6b) that the coagulation term is zero, i.e., coagulation preserves particle volume as it should.

Another observation is that (6a) and (6c) pose a closure problem, because they depend on unknown moments $M_{1/3}$, $M_{-1/3}$, $M_{4/3}$ and $M_{2/3}$. If we are to write the balance equations of those unknown moments, they will, in turn, depend on a new set of unknown moments, and so on, giving rise to an infinite system. In order to avoid this, we must be able to relate any required unknown moment to the set of known moments, i.e., the set of moments for which we are willing to solve a balance equation. There are several ways of doing this, like the quadrature method of moments [18] or the Presumed Number Density Function (PNDF) method. Here, we use the latter for its simplicity and ease of use. While presuming a certain number density function is often a crude simplification, the approach is justified here as we are after the identification of the main dynamics of the problem only.

2.2. Mono-dispersed closure

The most elementary PNDF assumes that the size distribution is mono-dispersed, i.e.,

$$n(v,t) = \delta(v - \overline{v})N, \tag{7}$$

with number concentration N and mean particle volume $\overline{v}$, which are the two unknowns of the PNDF and must be closed by retaining two moment balance equations. We select those of the number concentration and volume concentration. Introducing the PNDF in (4), we find

$$M_\gamma = \overline{v}^\gamma N, \tag{8}$$

which gives $M_0 = N$ and $M_1 = \overline{v}N = \overline{v}M_0$. In turn, we can relate M_γ to M_0 and M_1 by eliminating $\overline{v}$ from (8), giving

$$M_\gamma = M_0^{1-\gamma} M_1^\gamma. \tag{9}$$

We can use this relation to close (6a), resulting in

$$\frac{\mathrm{d}M_0}{\mathrm{d}t} = -2KM_0^2 + F, \tag{10}$$

which is the most elementary model for particle number evolution due to coagulation and formation. Together with (6b), it forms an uncoupled set of non-linear ordinary differential equations, which, subject to the initial condition $M_0(0) = 0$ and $M_1(0) = 0$, has solution

$$M_0(t) = \sqrt{F/(2K)}\tanh(\sqrt{2FK}t) \qquad \text{and} \qquad M_1(t) = wFt. \tag{11}$$

This outcome suggests that we can adopt the following non-dimensional quantities:

$$m_\gamma = \frac{M_\gamma}{w^\gamma\sqrt{F/K}} \qquad \text{and} \qquad \tau = \sqrt{FK}t, \tag{12}$$

with non-dimensional γth moment m_γ and non-dimensional time τ, turning the solution into

$$m_0(\tau) = \frac{\tanh(\sqrt{2}\tau)}{\sqrt{2}} \qquad \text{and} \qquad m_1(\tau) = \tau, \tag{13}$$

revealing the self-similarity of the problem as the solution is shaped independently of its parameters. From (13), we observe that for $\tau \to \infty$ the non-dimensional number concentration asymptotically approaches $1/\sqrt{2}$. In that limit, production by fission/decay is balanced by loss of number concentration by coagulation. Finally, the mean diameter of particles $\overline{d}$, related to the mean volume as $\overline{v} = \pi/6\,\overline{d}^3$, is then given by

$$\frac{\overline{d}}{b} = \sqrt[3]{\frac{\sqrt{2}\,\tau}{\tanh(\sqrt{2}\tau)}}, \tag{14}$$

with $b := \sqrt[3]{6w/\pi}$ the diameter of a single noble metal atom.

Fig. 1 shows the non-dimensional solution (14). It can be observed that from roughly one time unit onward the mean diameter linearly increases as a function of $\log(\tau)$, with slope $\frac{1}{3}$. This means that doubling of time is associated with only a $\sqrt[3]{2}$ increase in mean diameter. This result comes as no surprise, as we concluded that the number concentration asymptotically attains a constant value while particle volume increases at constant rate, indeed resulting in the slow particle growth as reflected by Fig. 1. What we learn from the above analysis is that particle growth is associated with a typical time $T_g = 1/\sqrt{FK}$, which we can compare to the macroscopic time scale of the reactor to obtain a first estimate of mean particle size. Roughly speaking, if T_g would be unity, then it takes minutes for particles to grow tenfold and days to grow hundredfold—if they were not to be removed from the system.

However, what we cannot extract from the above analysis is an estimate of the spread of particle sizes. In fact, for the mono-dispersed PNDF, all average diameters (like the count mean, count median, diameter of average mass, etc.) are the same. While the *count* mean particle diameter, which is represented from now on by $\overline{d}$, may be small, a wide particle spectrum will lead to a significant increase in other relevant mean diameters such as the *mass* mean diameter d_{mm}. For example, if the size distribution is log-normal, then the Hatch–Choate conversion equations [19] readily provide a relation between the count mean diameter and mass mean diameter, i.e.,

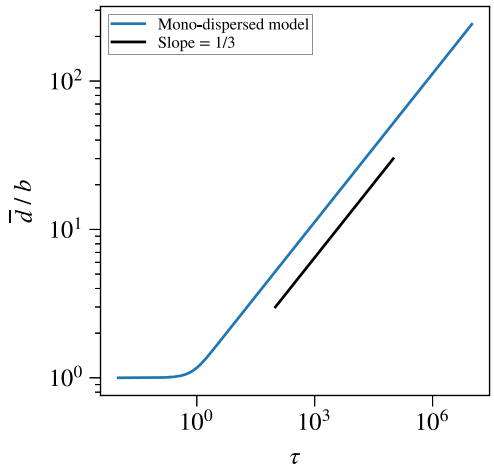

Fig. 1. Evolution of the non-dimensional mean particle diameter as a function of non-dimensional time, subject to the mono-dispersed PNDF.

$$d_{mm} = \overline{d}\exp(3\sigma^2), \tag{15}$$

with σ the logarithm of the geometric standard deviation. Thus, for a distribution with $\sigma = 1$, the mass mean diameter is roughly 20 times larger than the count mean diameter. Therefore, while the above analysis was useful in establishing the time scale of particle growth, we must extend it to include information on the variance of particle sizes.

2.3. Log-normal closure

A PNDF that is typically chosen is the log-normal size distribution, which was experimentally and numerically validated to be accurate in the context of particle coagulation [14]. Staying with a log-normal assumption, we replace the mono-dispersed PNDF by a distribution that is log-normal in diameter space. Writing that distribution in terms of volume space, we obtain [14]:

$$n(v,t) = \frac{N}{3\sqrt{2\pi}\sigma v}\exp\left(-\frac{\log^2(v/v_g)}{18\sigma^2}\right), \tag{16}$$

in which σ and N are as defined above and where v_g is the geometric number mean particle volume [19]. The log-normal size distribution is controlled by three parameters: height N, offset v_g and width σ. Introducing (16) into the definition of the γth moment (4), we find

$$M_\gamma = Nv_g^\gamma\exp\left(\frac{9}{2}\gamma^2\sigma^2\right) \tag{17}$$

Since the right-hand side has three unknown quantities, we must solve three independent moment equations and can then relate those moments to the arbitrary moment M_γ, in order to develop a closure relation. We select the number, volume and squared volume concentrations, giving

$$M_0 = N, \qquad M_1 = Nv_g\exp\left(\frac{9}{2}\sigma^2\right) \qquad \text{and} \qquad M_2 = Nv_g^2\exp\left(18\sigma^2\right). \tag{18}$$

Combining these to eliminate N, σ and v_g from (17), we obtain

$$M_\gamma^2 = \frac{M_0^{(\gamma-1)(\gamma-2)}M_2^{\gamma(\gamma-1)}}{M_1^{2\gamma(\gamma-2)}}. \tag{19}$$

This, then, is the log-normal closure relation that relates an arbitrary moment M_γ to the set of known moments (M_0, M_1, M_2), and can be used to close their respective balance equations. First, however, we non-dimensionalize the balance equations using the scaling given by (12), yielding

$$\frac{\mathrm{d}m_0}{\mathrm{d}\tau} = 1 - m_0^2 - m_{1/3}m_{-1/3}, \tag{20a}$$

$$\frac{\mathrm{d}m_1}{\mathrm{d}\tau} = 1 \tag{20b}$$

and

$$\frac{\mathrm{d}m_2}{\mathrm{d}\tau} = 1 + 2m_1^2 + 2m_{4/3}m_{2/3}. \tag{20c}$$

Eliminating the unknown moments with the non-dimensional equivalent of the log-normal closure relation (19), we find

$$\frac{\mathrm{d}m_0}{\mathrm{d}\tau} = 1 - m_0^2\left(1 + \sqrt[9]{q}\right), \tag{21a}$$

$$\frac{\mathrm{d}m_1}{\mathrm{d}\tau} = 1 \tag{21b}$$

and

$$\frac{\mathrm{d}m_2}{\mathrm{d}\tau} = 1 + 2m_1^2\left(1 + \sqrt[9]{q}\right), \tag{21c}$$

with the non-dimensional quantity q given by

$$q = \frac{m_0 m_2}{m_1^2}. \tag{22}$$

Using the non-dimensional equivalent of the definition of a log-normal moment, Eq. (17), we observe that

$$\sqrt[9]{q} = \exp(\sigma^2), \tag{23}$$

showing that for narrow size distributions with $\sigma \ll 1$ we have $\sqrt[9]{q} \approx 1$. The solution of (21a) is then approximated by (13). The equation of the volume moment remains unchanged and is therefore also provided by (13). In turn, assuming again that the q-term is close to unity, the right-hand side of (21c) can be approximated by $1 + 4m_1^2 = 1 + 4\tau^2$, giving the solution

$$m_2(\tau) = \tau + \frac{4\tau^3}{3}. \tag{24}$$

By definition, the diameter of average mass is given by

$$d_{\overline{m}} = b\sqrt[3]{\frac{6m_1}{\pi m_0}}. \tag{25}$$

From this, Eq. (23) and the Hatch–Choate relations, we can determine any mean diameter subject to the log-normal size distribution. For example, the count mean diameter is given by

$$\overline{d} = d_{\overline{m}}\exp(-\sigma^2) = b\sqrt[3]{6/\pi}\sqrt[9]{\frac{m_1^5}{m_0^4 m_2}} \sim \sqrt[9]{\tau^2}, \tag{26}$$

where the similarity with $\sqrt[9]{\tau^2}$ is obtained by substitution of the non-dimensional moments with their approximate solutions and taking the highest power in τ which will prevail in the limit of $\tau \to \infty$. Likewise, the mass mean diameter is given by

$$d_{mm} = d_{\overline{m}}\exp(2\sigma^2) = b\sqrt[3]{6/\pi}\sqrt[9]{\frac{m_2^2}{m_0 m_1}} \sim \sqrt[9]{\tau^5}. \tag{27}$$

This shows that the count mean diameter of the log-normal distribution grows slightly slower than the mean diameter in the mono-dispersed model (powers $\frac{2}{9}$ and $\frac{1}{3}$, respectively), but that the mass mean diameter grows quicker than both, with power $\frac{5}{9}$.

Fig. 2 (left) shows the approximate analytical solutions of the non-dimensional count mean diameter, mass mean diameter and diameter of average mass as a function of time, using the log-normal PNDF. As reference, also a numerical solution, in which the q-term is retained, is shown. The numerical solution is computed by application of the forward Euler scheme, and by applying the transformation $\tilde{t} = \log(\tau)$ which improves accuracy. The time step size $\Delta\tilde{t}$ is verified to be sufficiently small to establish numerical convergence, meaning that the numerical solution can be regarded as the exact solution. Appendix gives more details on the numerical algorithm to solve the set of equations. The numerical solution is very close to the approximate analytical one, demonstrating the validity of the latter. It can be observed in Fig. 2 that at about 10^3 time units the mass mean diameter is one order of magnitude larger than the count mean diameter, and has grown by two orders of magnitude. Fig. 2 (right) shows the non-dimensional size distribution at different non-dimensional times. The mass mean diameter position inside each distribution is marked. It can be seen that the number concentration at the position of the mass mean diameter is much smaller than the value at the peak of the distribution. Nevertheless, on average, mass is carried by particles that have a diameter equal to the mass mean one. Even though they are scarce, they contribute to transport of noble metal material most significantly.

3. Removal of particles by interfacial area

The Brownian diffusion of particles gives rise to agglomeration of them into larger particles. At the same time, the Brownian diffusion drives small particles to deposit onto interfaces such as those formed by bubbles. In the previous section, we have considered a situation without any depositories so that particles are free to grow without being removed from the system. This approach allowed us to study the typical dynamics of particle growth, and provided the relevant time scale of the problem along with an upper bound of particle sizes that can be expected to occur in the system at a given point in time, if no or very little interfacial area is present onto which particles can deposit and be removed, and if they are not removed by other means. In this section, we will study the rate at which particles are removed given the presence of an amount of interfacial area a_i, expressing the total area prone to deposition per unit volume present. We note that interfacial area can be expressed in terms of a combination of other moments of the bubble size distribution. For example, the product of mean bubble size squared and bubble number concentration equates to interfacial area up to a constant. However, ultimately it is the amount of depository area available to the particles that drives the removal of them by bubbles.

From nano-flotation theory, e.g., see [20], the sink term in the population balance equation modeling the diffusional removal of particles by interface is given by

$$\frac{\partial n(v,t)}{\partial t} = -\frac{\lambda a_i Kn(v,t)}{\sqrt[3]{v}}, \tag{28}$$

with λ the mass transfer coefficient in units of 1/m. The proportionality of the sink term to $1/\sqrt[3]{v}$ signifies that the particle diffusivity scales with $D \sim K/d$. The diffusivity D is ultimately driving the deposition rate, at least for small particles. As particles grow beyond 100 nm, they can also be transported to interfaces by different means such as sedimentation or inertial drift. However, to develop a first insight these mechanisms are ignored for now.

Again considering the number, volume and squared volume concentrations, (28) leads to

$$\frac{\mathrm{d}M_0}{\mathrm{d}t} = -BKM_{-1/3}, \quad \frac{\mathrm{d}M_1}{\mathrm{d}t} = -BKM_{2/3} \quad \text{and} \quad \frac{\mathrm{d}M_2}{\mathrm{d}t} = -BKM_{5/3}, \tag{29}$$

with $B = \lambda a_i$ which has units $1/\mathrm{m}^2$. Using the mono-dispersed closure, we find

$$\frac{\mathrm{d}M_0}{\mathrm{d}t} = -BKM_0\sqrt[3]{M_0/M_1} \quad \text{and} \quad \frac{\mathrm{d}M_1}{\mathrm{d}t} = -BKM_1\sqrt[3]{M_0/M_1} \tag{30}$$

The mathematical form of both equations in (30) is equivalent, implying that the solutions of M_0 and M_1 have a similarity in the sense of

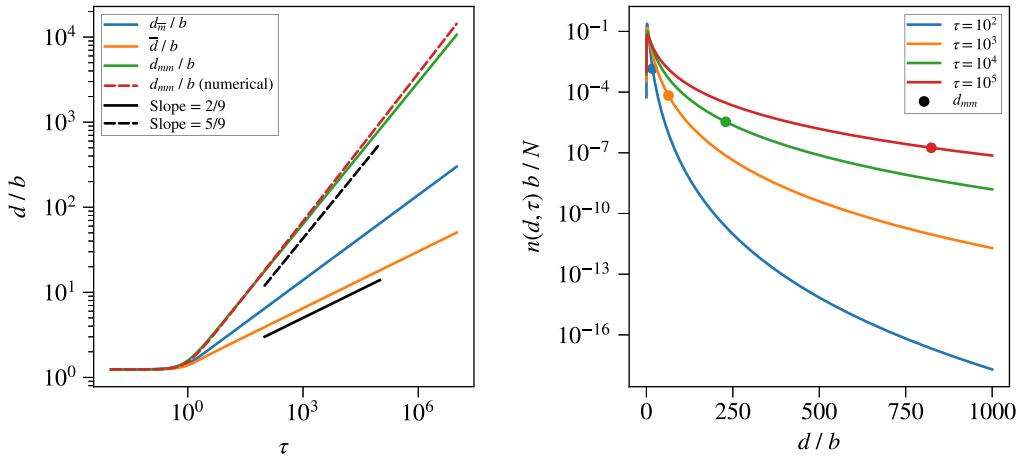

Fig. 2. Evolution of the diameter of average mass, count mean diameter and mass mean diameter as a function of time (left) and the size distribution at different non-dimensional times with the position of the mass mean diameter marked. Both graphs are calculated using the log-normal PNDF.

$M_0/M_1 = \text{const}$. Using this property, the solution to (30) is given by

$$M_0(t) = M_0(0)\exp\left(-BKt/\sqrt[3]{\overline{v}_0}\right) \quad \text{and} \quad M_1(t) = M_1(0)\exp\left(-BKt/\sqrt[3]{\overline{v}_0}\right), \tag{31}$$

where we use $\overline{v}_0 = M_1(0)/M_0(0)$ as the initial mean volume, which does not change in time for the mono-dispersed distribution. The solution suggests that the typical time of particle removal is $T_r = \sqrt[3]{w}/(BK)$. Using this as a scaling for time, and using any arbitrary scaling for the moments, the solution is given by

$$m_0(t) = m_0(0)\exp\left(-\frac{b\tau^\star}{\overline{d}_0}\right) \quad \text{and} \quad m_1(t) = m_1(0)\exp\left(-\frac{b\tau^\star}{\overline{d}_0}\right), \tag{32}$$

where $\tau^\star$ refers to the non-dimensional time of removal and $\overline{d}_0 = \sqrt[3]{6\,\overline{v}_0/\pi}$. The solution signifies that when the initial particle size becomes smaller, the removal is proportionally quicker.

In practice, particle spectra are not mono-dispersed so that the mean volume will change in time as small particles will be removed much quicker than larger ones. Thus, we would expect a gradual increase in mean particle sizes while the moments decrease exponentially. Using the log-normal closure in (29), we find

$$\frac{\mathrm{d}M_0}{\mathrm{d}t} = -BKM_0\sqrt[9]{\frac{M_0^5M_2^2}{M_1^7}}, \tag{33a}$$

$$\frac{\mathrm{d}M_1}{\mathrm{d}t} = -BKM_1\sqrt[9]{\frac{M_0^2}{M_1M_2}} \tag{33b}$$

and

$$\frac{\mathrm{d}M_2}{\mathrm{d}t} = -BKM_2\sqrt[9]{\frac{M_1^5}{M_0M_2^4}}. \tag{33c}$$

Indeed, these equations carry no similarity between themselves in the way that the mono-dispersed closure induced, making an analytical solution not immediately obvious. Instead, we solve the system numerically using the backward Euler scheme with a time step size sufficiently small to establish convergence. As above, the equations are numerically integrated not in time, but in the logarithm of time, which improves accuracy. See Appendix for more details. The model is made non-dimensional using $\tau^\star$ as the non-dimensional time and the scaling used in the previous section for the moments. This gives

$$\frac{\mathrm{d}m_0}{\mathrm{d}\tau^\star} = -m_0\sqrt[9]{\frac{m_0^5m_2^2}{m_1^7}}, \tag{34a}$$

$$\frac{\mathrm{d}m_1}{\mathrm{d}\tau^\star} = -m_1\sqrt[9]{\frac{m_0^2}{m_1m_2}} \tag{34b}$$

and

$$\frac{\mathrm{d}m_2}{\mathrm{d}\tau^\star} = -m_2\sqrt[9]{\frac{m_1^5}{m_0m_2^4}}. \tag{34c}$$

Fig. 3 (left) shows the time evolution of the non-dimensional moments, scaled by their respective initial values, for a log-normal distribution of which the initial count mean diameter $\overline{d}_0$ is $20b$ and which has a moderate width $\sigma = \frac{1}{2}$. Also shown is the mono-dispersed solution for m_0 and m_1, also scaled by their respective initial values and with the same ratio $\overline{d}_0/b$. The removal of particles is most pronounced for the number concentration moment, which is more strongly associated with the behavior of small particles. Initially, its decay is faster for the log-normal PNDF as compared to the mono-dispersed PNDF, as the log-normal distribution contains many small particles which are quickly removed leading to, in turn, an increase in mean particle size. However, the removal of small particles does not remove mass from the system very efficiently. The volume concentration is seen to decrease slower for the log-normal PNDF than that for the mono-dispersed one. This demonstrates that modeling of the complete size distribution is relevant in the calculation of removal rates, and that a mono-dispersed assumption can be deceiving. Fig. 3 (right) shows the evolution of non-dimensional average diameters for the same initial log-normal distribution subject to particle removal. As expected, mean diameters are seen to increase as a result of smaller particles being removed quickest.

4. Noble metal particle size spectra with both source and sink

The previous two sections have identified two typical times, i.e., the typical time of particle growth T_g and the typical time of particle removal T_r. These two time scales control the problem which, when $T_g \ll T_r$ or $T_g \gg T_r$, is multi-scale. In the first inequality we have fast particle growth producing large particles while in the second we have efficient removal of particles such that they do not grow to be large. In this section, we will combine the models for growth and removal and study the dependence of the result on its parameters.

4.1. Combined model for particle growth and removal

Continuing with the log-normal PNDF, the model for particle growth is given by (21) and the model for particle removal by (34). The time scale of both sets of equations differs by a factor $\Pi = T_g/T_r$, and are thus readily combined into

$$\frac{\mathrm{d}m_0}{\mathrm{d}\tau} = 1 - m_0^2\left(1 + \sqrt[9]{q}\right) - \Pi\, m_0\sqrt[9]{\frac{m_0^5m_2^2}{m_1^7}}, \tag{35a}$$

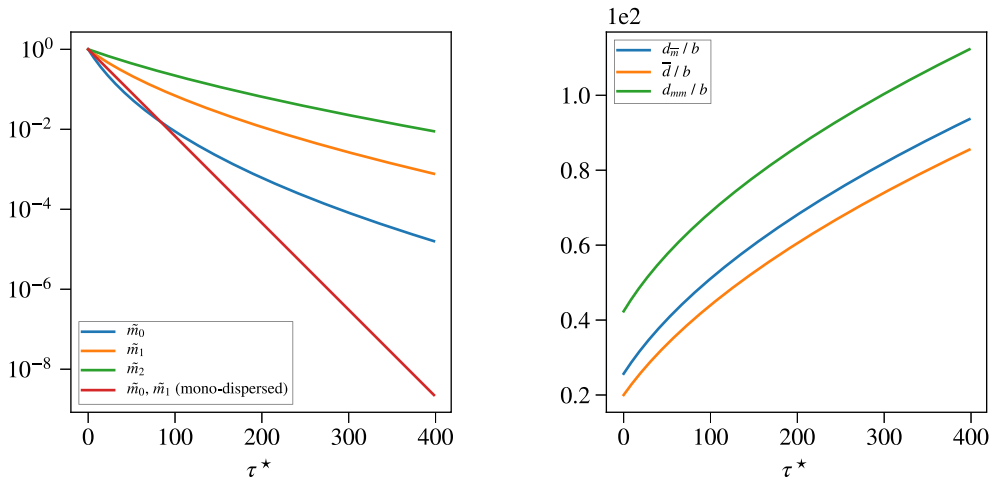

Fig. 3. Time evolution of the non-dimensional moments scaled by their initial value (left) and non-dimensional diameters (right), for a log-normal distribution of which the initial count mean diameter $\overline{d}_0$ is $20b$ and which has a moderate width of $\sigma = \frac{1}{2}$. Also shown are the solutions for the first two moments using the mono-dispersed PNDF. The scaling of non-dimensional moments by their initial value is denoted with the tilde.

$$\frac{\mathrm{d}m_1}{\mathrm{d}\tau} = 1 - \Pi\, m_1 \sqrt[9]{\frac{m_0^2}{m_1 m_2}} \tag{35b}$$

and

$$\frac{\mathrm{d}m_2}{\mathrm{d}\tau} = 1 + 2m_1^2\left(1 + \sqrt[9]{q}\right) - \Pi\, m_2 \sqrt[9]{\frac{m_1^5}{m_0 m_2^4}}, \tag{35c}$$

where we recall that $q = m_0 m_2 / m_1^2$. Clearly, for $\Pi \to 0$, growth is much quicker than removal and (35) reduces to (21). Conversely, for $\Pi \to \infty$ removal is much quicker than growth and (35) reduces to (34) instead. Thus, the equilibrium solution for $\tau \to \infty$ is only a function of Π. Introducing the definitions of T_g, T_r and B, we find

$$\Pi = \frac{T_g}{T_r} = \frac{\lambda a_i}{b}\sqrt{\frac{K}{F}}. \tag{36}$$

Fig. 4 (top left) shows the time evolution of the non-dimensional mass mean diameter for a range of values of Π. The solution was numerically calculated using the same approach as before, where the source terms are treated using the forward Euler scheme and the sink terms using the backward Euler scheme, the latter for stability. Again, a logarithmic transformation of time is applied to achieve better accuracy. See Appendix for more details. For the largest value of Π shown in Fig. 4 (top left), the equilibrium distribution is attained quickly at relatively low mass mean diameter. For smaller values of Π, a successive increase in both the time needed to achieve steady state as well as the mass mean diameter at equilibrium, is observed. Fig. 4 (top right) shows how the equilibrium mean diameters are a function of the reciprocal of Π, with a linear dependence being observed. A first order polynomial fit shows that $d_{\overline{m}} \sim 1/\Pi^{0.74}$, $\overline{d} \sim 1/\Pi^{0.35}$ and $d_{mm} \sim 1/\Pi^{1.5}$. Fig. 4 (bottom) shows the equilibrium size distributions for a range of values of Π, that is obtained by evaluation of Eq. (16) using (23) for σ and (17) for v_g evaluated for $\gamma = 2$.

We conclude from these results that in order to establish a size distribution of noble metal particles with particle sizes reaching the micrometer scale, we have two requirements. First, the non-dimensional number Π must be smaller than unity. As can be seen from the definition of Π, Eq. (36), this can be realized by having a small interfacial area concentration, a small coagulation constant K or a large noble metal particle production rate F. Second, the system must be given sufficient time to evolve, for particles to grow substantially. The typical time of growth, given by $T_g = 1/\sqrt{FK}$, must thus be much smaller than the macroscopic time scale of the system, e.g., the time of operation of the reactor. Small time scales for growth are established by a large noble metal particle production rate F or large coagulation constant K. This latter observation is opposed by the requirement for small Π, which demands a small coagulation constant K.

Finally, another relevant quantity to analyze is the typical time of removal of particles, i.e., the *cycle time* constant τ_c. The cycle time is a measure for how quickly noble metal mass is extracted by bubbles and removed from the system. At equilibrium, the rate of removal is balanced by the rate of production, so that there is no net removal of mass. If we were to instantly stop particle formation at equilibrium, then the particle mass would slowly be removed by bubbles and decay in time. The time scale contained in this particle mass decay function is representative of the cycle time. Without any particle formation, the balance equation of the volume moment (35b), which is representative of particle mass up to a constant factor of mass density, is given by

$$\frac{\mathrm{d}m_1}{\mathrm{d}\tau} = -s\Pi m_1 \qquad \text{with} \qquad s = \sqrt[9]{\frac{m_0^2}{m_1 m_2}}. \tag{37}$$

The factor s will vary only weakly due its power $\frac{1}{9}$. If we approximate s as a constant, then its solution (scaled by its initial value) is given by $\tilde{m}_1(\tau) = \exp(-s\Pi\tau)$, from which we infer that the cycle time is given by $\tau_c = 1/(s\Pi)$, with s calculated from the equilibrium values of the three moments. Fig. 5 shows the cycle time for a range of values of Π, directly calculated from the solutions presented in Fig. 4. The trend is linear in the double logarithmic plot, suggesting that a first order polynomial fit matches the solution well. Such a fit is shown in Fig. 5, and is described by

$$\tau_c = 2.02/\Pi^{2.12}, \tag{38}$$

i.e., the dependence of the cycle time on Π is close to inversely quadratic. Note that τ_c is non-dimensional and scaled by T_g.

4.2. Application to the MSFR

In order to calculate estimates of actual size distributions in the MSFR [2], we must specify the time scale of growth, T_g, and the time scale of removal, T_r. Estimates of the relevant quantities for the MSFR are shown in Table 1 and are mainly taken from [21,22]. The noble metal particle production rate is based on a benchmark simulation of the MSFR inventory. The total number of noble metal atoms present at equilibrium was taken, and divided by the cycle time of noble metal removal that was used in the simulation, which equaled 30 s. The initial particle diameter, being the average atomic diameter, is a rough estimate but should reasonably represent the order of magnitude. Also the bubble diameter is not known, but we will study the sensitivity of the model to this parameter later and initially assume it is 1 mm, which should also reasonably reflect its order of magnitude and is in agreement with that chosen by Caruggi et al. [23].

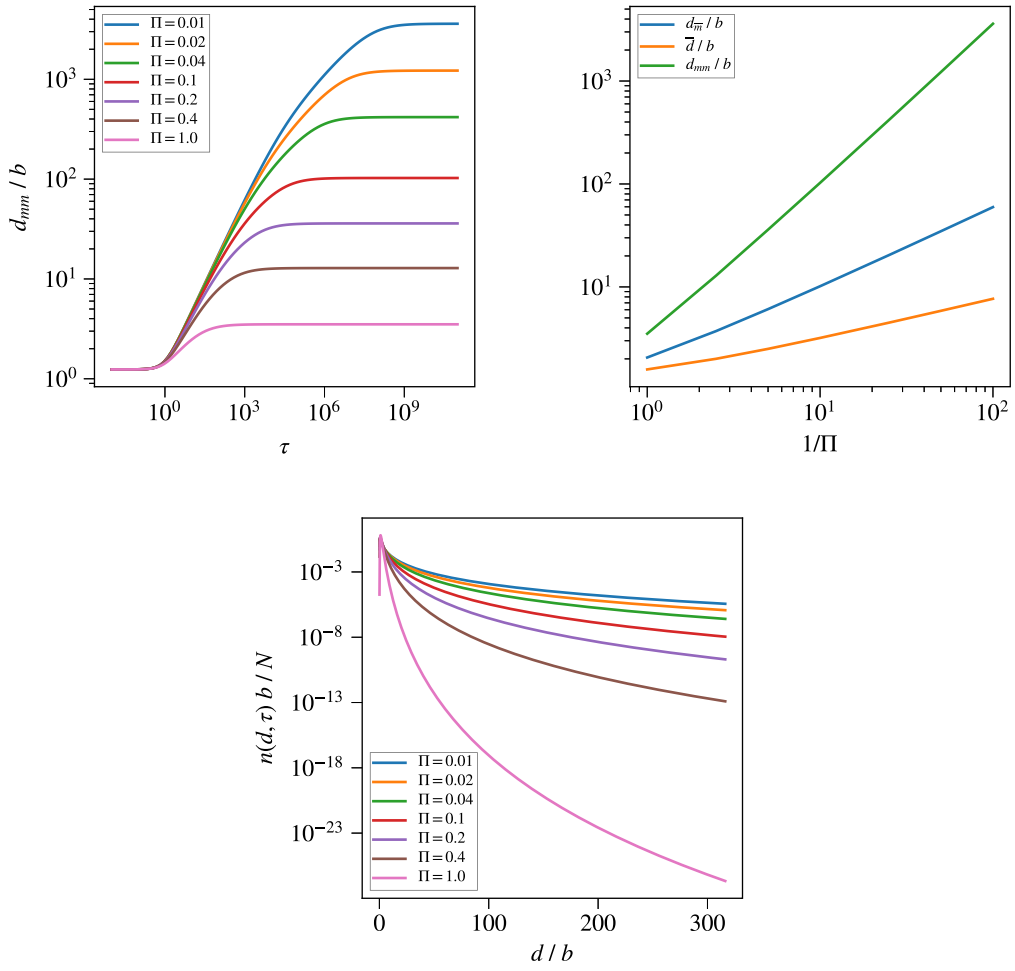

Fig. 4. Top left: time evolution of the non-dimensional mass mean diameter for a range of values of Π. Top right: equilibrium mass mean diameter as a function of $1/\Pi$. Bottom: size distribution of particles at equilibrium for a range of values of Π.

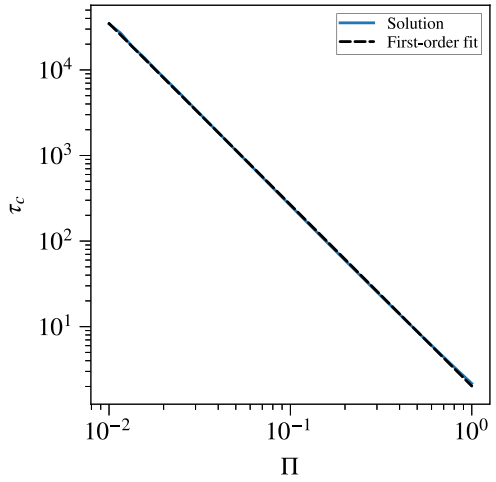

Fig. 5. The non-dimensional cycle time as a function of Π.

Table 1
Estimate of the values of key parameters of the MSFR, controlling the shape of the noble metal particle spectrum. Void fraction α has been left undefined.

Quantity	Value
Particle production rate F	2.2×10^{18} 1/m^3/s
Salt temperature T	1000 K
Salt dynamic viscosity μ	0.01 kg/m/s
Salt mass density ρ	4215 kg/m^3
Helium mass density ρ_b	0.048 kg/m^3
Initial particle diameter b	1 Å
Salt volume V	18 m^3
Bubble diameter d_b	1 mm
Calculated values	
Coagulation constant K	9.2×10^{-19} m^3/s
Particle Schmidt number Sc	1.6×10^6
Bubble Reynolds number Re	35
Sherwood number Sh	421
Removal coefficient B	$[4.02\times10^8$ m$^{-2}]\times\alpha$
Resulting time scales	
Time scale of growth T_g	0.703 s
Time scale of removal T_r	[0.270 s]/α
Non-dimensional parameter Π	$2.60\times\alpha$
Non-dimensional cycle time τ_c	$2.02/(2.60\times\alpha)^{2.12}$
Cycle time T_c	$0.703\times\tau_c$ s

The volume flow of bubbles, controlling the void fraction α, is an operational parameter that can be leveraged to achieve optimal particle removal. We note, however, that when bubbling is applied directly to the reactor core, high voids in the system can lead to problems with reactivity control, so the volumetric flow of bubbles will have an upper limit set by neutronic considerations. The parameter B is related to the product of the interfacial area and the mass transfer coefficient. For

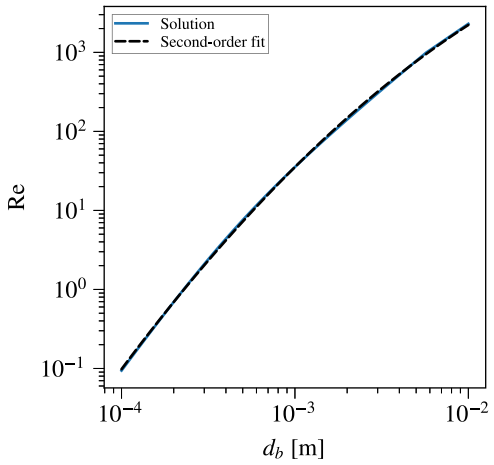

Fig. 6. Numerical solution and fit (according to (44)) of the dependence of the bubble Reynolds number on bubble diameter.

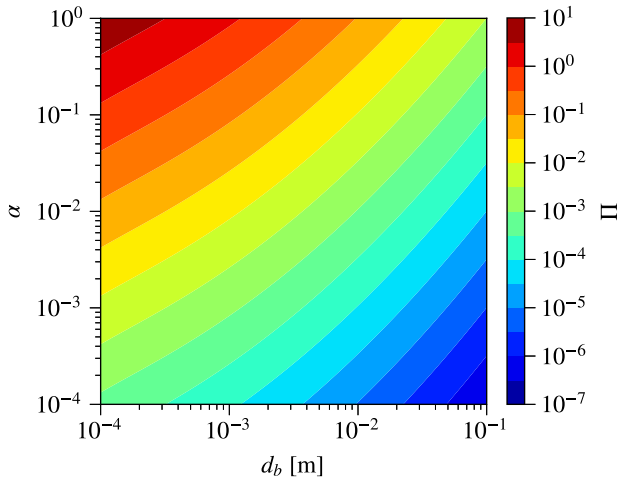

Fig. 7. Dependence of the non-dimensional parameter Π on the void fraction and bubble diameter.

diffusional flotation of particles by bubbles, we have

$$\lambda = \frac{\mathrm{Sh}}{2\pi d_b} \tag{39}$$

with Sauter mean bubble diameter d_b and Sherwood number Sh. The Sauter mean diameter satisfies the relation

$$a_i = \frac{6\alpha}{d_b}, \tag{40}$$

which results in

$$B = \lambda a_i = \frac{3\mathrm{Sh}\alpha}{\pi d_b^2}, \tag{41}$$

showing that B strongly depends the bubble diameter. For the Sherwood correlation of bubbles, we leverage the analogy with heat and mass transfer that was observed in the MSRE experiments, such that it is given by the Ranz–Marshall [24] correlation, i.e.,

$$\mathrm{Sh} = 2 + 0.6\sqrt{\mathrm{Re}}\sqrt[3]{\mathrm{Sc}}, \tag{42}$$

with bubble Reynolds number Re and Schmidt number Sc.

The Reynolds number is defined as $\mathrm{Re} = |\mathbf{u}_r| d_b \rho/\mu$ with $\mathbf{u}_r$ the relative velocity between bubbles and salt, which is a function of the bubble size. The magnitude of the relative velocity can be estimated well by the equilibrium bubble rise velocity U resulting from a balance between gravity and drag, i.e.,

$$\left(\frac{\rho}{\rho_b} - 1\right) g = \frac{C_d \mathrm{Re}}{24\tau_{\mathrm{St}}} U, \tag{43}$$

with bubble mass density ρ_b, gravity g, drag coefficient C_d and Stokes relaxation time $\tau_{\mathrm{St}} = \rho_b d_b^2/(18\mu)$. For spherical bubbles, the drag coefficient is given by the Schiller–Naumann correlation, e.g., see [25]. It is a non-linear function of the bubble Reynolds number, and holds for spherical bubbles having Reynolds numbers below 10^3 [25]. It is expected that this shall be the case in the MSFR, although we note that other drag correlations may be readily used too. Eq. (43), subject to its parameters as reported in Table 1, can be solved for U numerically using a simple iterative scheme, for a range of bubble diameters. In turn, the solution for U provides the Reynolds number as function of d_b. Fig. 6 shows the solution for Re for bubbles in the size range of 0.1 mm to 1 cm. The solution appears as a mildly curved line in the double logarithmic plot, which suggests that a second order polynomial regression in that space is accurate. Such a regression is shown in Fig. 6. It is given by

$$\log(\mathrm{Re}) = 10.74 - 0.1009\log(d_b) - 0.1649\log^2(d_b). \tag{44}$$

This function can be conveniently used to estimate the bubble Reynolds number, and is applicable to the conditions of the MSFR. For bubbles of 1 mm, the Reynolds number is about 35.

The Schmidt number is defined as $\mathrm{Sc} = \mu/(\rho D)$ and is, through D, a function of the particle diameter. This complicates the situation somewhat, as it makes the parameter B, through Sh, a function of particle diameter and can therefore not be assumed constant, as was done in the previous sections. However, this dependence is quite weak because in the limit of large Sc we have $\mathrm{Sh} \sim \sqrt[3]{\mathrm{Sc}} \sim \sqrt[3]{1/D} \sim \sqrt[3]{d}$. Thus, on a large particle size range of three decades, the Schmidt number will only vary by a factor 10. Subsequently, we compute the Schmidt number based on a particle diameter of 100 nm. Given the parameters in Table 1, its value is $\mathrm{Sc} = 1.6{\times}10^6$. This gives, for bubbles with a diameter of 1 mm, a Sherwood number of $\mathrm{Sh} = 421$.

With these values, we obtain the time scales and non-dimensional parameters as listed at the bottom of Table 1. At void fractions of $\mathcal{O}(10^{-2})$, the value of Π is still quite low suggesting that if particle agglomeration is to establish equilibrium, then large particles will arise in the process, growing significantly towards the micrometer scale. However, this is only likely to occur at large time scales, see Fig. 4. The typical time of growth, with which time is made non-dimensional in this Figure, is in the order of 1 s, so that when Π is around 4×10^{-2} (corresponding to a void fraction of about 1.5%), it would require minutes to form particles with a mass mean diameter in the order of tens of nanometers and days to reach beyond hundreds of nanometers. Finally, the non-dimensional cycle time at the same value for Π is 1858, and the dimensional cycle time is about 22 min. Note that a void fraction twice as high will decrease the cycle time more than fourfold, thus achieving much higher removal rates.

Fig. 7 shows the dependence of the non-dimensional parameter Π on the void fraction and the bubble diameter. The dependence on the void fraction is linear, but the dependence on the bubble diameter is more complicated through the non-linear dependence of the bubble Reynolds number on the bubble diameter. It is shown that for bubbles of 1 mm, void fractions beyond 10% will result in small particle growth with Π approaching unity. For significantly larger bubbles, the value of Π will always be much smaller than unity assuring that particle growth will be substantial, for the considered reactor parameters. For very fine bubbles, relatively small void fractions are needed to achieve limited particle growth. For example, 1 cm bubbles at about 10% void fraction will achieve the same equilibrium particle distribution as 0.1 mm bubbles will at just 0.1% void fraction. This encourages an MSR design with a bubbling system that produces small bubbles, to keep void fractions low. However, we note that turbulent bubble coalescence

and break-up tend to drive bubble populations to a mean diameter that is independent of inlet conditions.

Thus far, we have only considered removal of particles by bubbles. The model can be easily extended to include a sink term which captures removal of particles by wall deposition. In short, a second sink term should be added with a proportionality to the mass transfer coefficient of the wall and the interfacial area concentration of the wall. However, the interfacial area concentration of the wall is likely to be smaller than that presented by bubbles, as already explained in the introduction. An increase of the reactor volume will further decrease the interfacial area concentration of the wall, while the bubbly interfacial area concentration (at uniform void fraction) remains the same. Thus, with the MSFR salt volume of about 18 m^3, the total area of depositories is likely to be predominantly that of bubbles. This makes the above analysis applicable to reactors with walls.

5. Conclusions

In this work, we studied the formation and removal of noble metal particles in an MSR by considering particle kinetics in a homogeneous reactor. The only considered mechanism of removal was that by bubbles, through diffusional nano-flotation. It was assumed that noble metal atoms do not decay, or only decay into other noble metal atoms, therewith keeping the noble metal mass roughly constant. A population balance equation, describing the evolution of noble metal agglomerates, was solved using the method of moments. More specifically, the log-normal PNDF was used to close a set of three moment equations. While this reduces the complexity of the model significantly, it preserves the fundamental dynamics inherent to the problem and thus provides estimates of the scales involved in the process. The problem is essentially governed by the parameter Π which is the ratio of the time scale of growth by coagulation and time scale of removal by flotation. On one hand, small values of Π lead to rapid particle growth, yielding an equilibrium particle size distribution containing large particles up to, or even beyond, the micrometer scale. This would invoke a transition from diffusional flotation to hydrodynamic flotation. However, it was shown that the time to establish equilibrium also increased proportionally to the reciprocal of Π, suggesting that large particles can only be significantly generated in the reactor at long operational times. On the other hand, large values of Π lead to an efficient particle removal by flotation and limit the growth of particles significantly.

The parameter Π is proportional to the interfacial area concentration, the square root of the coagulation constant and the square root of the reciprocal of the formation rate of noble metal atoms. The coagulation constant and formation rate are properties subject to the operational conditions of the reactor, and cannot be easily controlled. To the contrary, the interfacial area concentration can be easily manipulated by controlling the flow of bubbles. The interfacial area concentration is directly related to the void fraction, which, in turn, is proportional to Π. Thus, through the developed theory, we can readily deduce the behavior of noble metal particles solely from the void fraction. For example, in the MSFR a void fraction of 1% of 1 mm bubbles would give a cycle time of roughly one hour and would produce particles with a mass mean diameter of about 200 nm. However, it would require years of steady-state operation to achieve such particle sizes. A doubling of the void fraction would reduce the cycle time to about 15 min and decrease the mass mean diameter to just 60 nm which would be achieved in a matter of months of steady-state operation.

To develop the theory, a number of simplifications were made. First, the reactor was assumed to be completely homogeneous without any walls. Particle removal was modeled to only occur by deposition onto bubbles. In practice, however, particles will also deposit onto the walls of the reactor vessel and probably more so on the large surface of the heat exchanger, potentially amplified by thermophoresis. The influence of solid walls on the particle population can be integrated into the presented model by including another sink term which will depend on the interfacial area concentration of the wall and a suitable model for the mass transfer coefficient. Noble metals can also be removed by decay, which can potentially also be accommodated in the presented model. What cannot be implemented easily in the model, on the other hand, is the non-uniformity of the flow in an MSR, which will affect the coagulation and mass transfer processes, as well as the behavior of bubbles subject to turbulent coalescence and break-up, and expansion as they rise to the top of the reactor vessel or as the result of local temperature changes. Such spatial effects can only be considered using advanced computational fluid dynamics codes, and must be assessed quantitatively. Once the fully detailed spatial behavior of the bubble size distribution, subject to coalescence, break-up, pressure or temperature changes, is known, an appropriate spatial averaging technique should be used to calculate the mean bubble size that can then act as input to the present model. This is part of ongoing work.

A major challenge that remains is the appropriate validation of the present model, under relevant conditions. This would require experiments that operate using real molten salts subjected to neutron irradiation, in order to produce realistic fission rates of noble metal atoms. Nevertheless, the theory developed in this work contributes significantly to a qualitative understanding of the behavior of noble metals in an MSR which, as a result of the complex interplay of formation, coagulation and flotation, is certainly non-trivial. The theory can potentially help to explain certain phenomena observed in the MSRE and can assist in the future design of noble metal flotation experiments and, eventually, safe and reliable MSRs.

Funding

This project has received funding from the Euratom research and training program 2019–2023, under grant agreement No. 847527.

Disclaimer

The content of this paper does not reflect the official opinion of the European Union. Responsibility for the information and/or views expressed therein lies entirely with the authors.

CRediT authorship contribution statement

E.M.A. Frederix: Conceptualization, Methodology, Software, Formal analysis, Writing – original draft, Writing – review & editing.

Declaration of competing interest

The authors declare that they have no known competing financial interests or personal relationships that could have appeared to influence the work reported in this paper.

Data availability

No data was used for the research described in the article.

Appendix. Numerical solution algorithm for a general system of moment equations

If we let $\mathbf{m} \in \mathbb{R}^n$ be a vector of n scalar moments, then we can generally write the non-linear system of coupled moment equations as

$$\frac{\mathrm{d}\mathbf{m}}{\mathrm{d}\tau} = \mathbf{A}\mathbf{m} + \mathbf{f}, \tag{45}$$

where the right-hand side is split into a part that is proportional to $\mathbf{m}$ with coefficient matrix $\mathbf{A} \in \mathbb{R}^{n\times n}$ a function of $\mathbf{m}$, and a remainder $\mathbf{f} \in \mathbb{R}^n$ that is a function of $\mathbf{m}$ too. As we will see below, by making

this split we can apply a mixed form of forward and backward Euler discretization which will guarantee positivity of the moments and, thus, promote stability. While not a strict requirement, it is convenient to let $\mathbf{A}$ be a diagonal matrix, such that the first term in the right-hand side introduces no coupling between moments. This can always be enforced by the choice for $\mathbf{f}$.

The solution to Eq. (45) is likely to introduce exponential behavior as a result of its non-linearity. Therefore, it is numerically advantageous to apply the transformation

$$x = {}^{10}\log(\tau) \qquad \Longleftrightarrow \qquad \tau = 10^{x} \tag{46}$$

which assures that time increases with powers of x. The modified system becomes

$$\frac{1}{T}\frac{\mathrm{d}\mathbf{m}}{\mathrm{d}x} = \mathbf{A}\mathbf{m} + \mathbf{f}. \tag{47}$$

with $T = \log(10)\tau$. Applying a backward Euler discretization to the first right-hand side term and a forward Euler discretization to the second, with numerical time step size Δx, we find

$$\frac{\mathbf{m}^{i+1} - \mathbf{m}^{i}}{\Delta x} = T\left(\mathbf{A}^{i}\mathbf{m}^{i+1} + \mathbf{f}^{i}\right), \tag{48}$$

or,

$$\mathbf{m}^{i+1} = \left(\mathbf{I} - T\Delta x\mathbf{A}^{i}\right)^{-1}\left(\mathbf{m}^{i} + T\Delta x\mathbf{f}^{i}\right), \tag{49}$$

with $\mathbf{I}$ the $n \times n$ identity matrix and where the superscripts signify the discrete time step number $i \in (0, 1, \dots)$. If we choose $\mathbf{A}$ and $\mathbf{f}$ in such a way that the diagonal components of $\mathbf{A}$ satisfy $A_{jj} \leq 0$, and that the source term components satisfy $f_j \geq 0$, then the iterative Eq. (49) trivially reveals that it preserves positivity of the moments, i.e., $m_j^i \geq 0$ for all i, j.

Using Eq. (49), the discrete solution of (45) is obtained by recursion, with initial value $\mathbf{m}^0 = 0$. The initial value for the power x is set to -2, which corresponds to 0.01 time units, and it was found that a value of $\Delta x = 1/20$, resulting in 20 steps per time unit decade, was sufficient for numerically converged results. The final value for the power x was set according to the dynamics of the system at hand.

References

[1] J. Serp, M. Allibert, O. Beneš, S. Delpech, O. Feynberg, V. Ghetta, D. Heuer, D. Holcomb, V. Ignatiev, J.L. Kloosterman, et al., The molten salt reactor (MSR) in generation IV: Overview and perspectives, Prog. Nucl. Energy 77 (2014) 308–319.

[2] E. Merle-Lucotte, D. Heuer, M. Allibert, M. Brovchenko, N. Capellan, V. Ghetta, Launching the thorium fuel cycle with the molten salt fast reactor, in: Proceedings of ICAPP, Vol. 2, 2011.

[3] R.J. Kedl, Migration of a Class of Fission Products (Noble Metals) in the Molten-Salt Reactor Experiment, Technical Report, Oak Ridge National Lab., Tenn.(USA), 1972.

[4] F.N. Peebles, Removal of Xe-135 from circulating fuel salt of the MSBR by mass transfer to helium bubbles, 1968, Oak Ridge National Lab..

[5] W.R. Grimes, Molten-salt reactor chemistry, Nucl. Appl. Technol. 8 (2) (1970) 137–155.

[6] E.L. Compere, S.S. Kirslis, E.G. Bohlmann, F.F. Blankenship, W.R. Grimes, Fission Product Behavior in the Molten Salt Reactor Experiment, Technical Report, Oak Ridge National Lab.(ORNL), Oak Ridge, TN (United States), 1975.

[7] S. Delpech, E. Merle-Lucotte, D. Heuer, M. Allibert, V. Ghetta, C. Le-Brun, X. Doligez, G. Picard, Reactor physic and reprocessing scheme for innovative molten salt reactor system, J. Fluor. Chem. 130 (1) (2009) 11–17.

[8] M.W. Rosenthal, R.B. Briggs, P.R. Kasten, Molten-Salt Reactor Program Semiannual Progress Report for Period Ending February 28, 1969, Technical Report, Oak Ridge National Lab.(ORNL), Oak Ridge, TN (United States), 1969.

[9] A.V. Nguyen, H.J. Schulze, Colloidal Science of Flotation, Vol. 118, CRC Press, 2003.

[10] A.V. Nguyen, P. George, G.J. Jameson, Demonstration of a minimum in the recovery of nanoparticles by flotation: Theory and experiment, Chem. Eng. Sci. 61 (8) (2006) 2494–2509.

[11] S.K. Friedlander, Smoke, Dust and Haze: Fundamentals of Aerosol Behavior, Wiley-Interscience, New York, 1977.

[12] R.L. Drake, The scalar transport equation of coalescence theory: Moments and kernels, J. Atmos. Sci. 29 (3) (1972) 537–547.

[13] K.W. Lee, H. Chen, Coagulation rate of polydisperse particles, Aerosol Sci. Technol. 3 (3) (1984) 327–334.

[14] K.W. Lee, J. Chen, J.A. Gieseke, Log-normally preserving size distribution for Brownian coagulation in the free-molecule regime, Aerosol Sci. Technol. 3 (1) (1984) 53–62.

[15] F. Gelbard, J.H. Seinfeld, Simulation of multicomponent aerosol dynamics, J. Colloid Interface Sci. 78 (2) (1980) 485–501.

[16] S. Kumar, D. Ramkrishna, On the solution of population balance equations by discretization–I. A fixed pivot technique, Chem. Eng. Sci. 51 (8) (1996) 1311–1332.

[17] E.M.A. Frederix, Eulerian Modeling of Aerosol Dynamics (Ph.D. thesis), University of Twente, 2016.

[18] R. McGraw, Description of aerosol dynamics by the quadrature method of moments, Aerosol Sci. Technol. 27 (2) (1997) 255–265.

[19] W.C. Hinds, Aerosol Technology: Properties, Behavior, and Measurement of Airborne Particles, John Wiley & Sons, 2012.

[20] N. Mishchuk, J. Ralston, D. Fornasiero, The analytical model of nanoparticle recovery by microflotation, Adv. Colloid Interface Sci. 179 (2012) 114–122.

[21] M. Aufiero, A. Cammi, C. Fiorina, J. Leppänen, L. Luzzi, M.E. Ricotti, An extended version of the SERPENT-2 code to investigate fuel burn-up and core material evolution of the molten salt fast reactor, J. Nucl. Mater. 441 (1–3) (2013) 473–486.

[22] M. Aufiero, A. Cammi, O. Geoffroy, M. Losa, L. Luzzi, M.E. Ricotti, H. Rouch, Development of an OpenFOAM model for the molten salt fast reactor transient analysis, Chem. Eng. Sci. 111 (2014) 390–401.

[23] F. Caruggi, A. Cammi, E. Cervi, A. Di Ronco, S. Lorenzi, Multiphysics modelling of gaseous fission products in the molten salt fast reactor, Nucl. Eng. Des. 392 (2022) 111762.

[24] W.E. Ranz, W.R. Marshall, Evaporation from drops, Chem. Eng. Prog. 48 (3) (1952) 141–146.

[25] R. Clift, J.R. Grace, M.E. Weber, Bubbles, Drops, and Particles, Courier Corporation, 2005.